Research Article | Vol. 9, No. 3 | 1 Mar 2018 | BIOMEDICAL OPTICS EXPRESS 921
Biomedical Optics EXPRESS

Optical properties of acute kidney injury measured by quantitative phase imaging

SUNGBEA BAN,[1,5] EUNJUNG MIN,[2,5] SONGYEE BAEK,[1] HYUG MOO KWON,[3] GABRIEL POPESCU,[4,6] AND WOONGGYU JUNG[1,7]

[1]*Department of Biomedical Engineering, Ulsan National Institute of Science and Technology (UNIST), Ulsan, South Korea*
[2]*Rowland Institute, Harvard University, Boston, Massachusetts, USA*
[3]*Department of Biological Science, Ulsan National Institute of Science and Technology (UNIST), Ulsan, South Korea*
[4]*Quantitative Light Imaging Laboratory, Department of Electrical and Computer Engineering, Beckman Institute for Advanced Science and Technology, University of Illinois at Urbana-Champaign, Urbana, Illinois 61801, USA*
[5]*These authors contributed equally to this work*
[6]*gpopescu@illinois.edu*
[7]*wgjung@unist.ac.kr*

Abstract: The diagnosis of acute kidney disease (AKI) has been examined mainly by histology, immunohistochemistry and western blot. Though these approaches are widely accepted in the field, it has an inherent limitation due to the lack of high-throughput and quantitative information. For a better understanding of prognosis in AKI, we present a new approach using quantitative phase imaging combined with a wide-field scanning platform. Through the phase-delay information from the tissue, we were able to predict a stage of AKI based on various optical properties such as light scattering coefficient and anisotropy. These optical parameters quantify the deterioration process of the AKI model of tissue. Our device would be a very useful tool when it is required to deliver fast feedback of tissue pathology or when diseases are related to mechanical properties such as fibrosis.

OCIS codes: (180.3170) Interference microscopy; (120.5050) Phase measurement; (160.4760) Optical properties; (290.5820) Scattering measurements; (110.3080) Quantitative phase imaging.

References and links

1. P. Glover, and P. Mansfield, "Limits to magnetic resonance microscopy," Rep. Prog. Phys. **65**, 1489 (2002).
2. A. Garcia-Sanz, A. Rodriguez-Barbero, M. D. Bently, E. L. Ritman, and J. C. Romero, "Three-dimensional micro-copmuted tomography of renal vasculature in rats," Hypertension **31**(440 (1998).
3. G. C. Gobe, N. C. Bennett, M. West, P. Colditz, L. Brown, D. A. Vesey, and D. W. Johnson, "Increased progression to kidney fibrosis after erythropoietin is used as a treatment for acute kidney injury," Am. J. Physiol. Renal Physiol. **306**(6), F681–F692 (2014).
4. Y. Chen, P. M. Andrews, A. D. Aguirre, J. M. Schmitt, and J. G. Fujimoto, "High-resolution three-dimensional optical coherence tomography imaging of kidney microanatomy ex vivo," J. Biomed. Opt. **12**(3), 034008 (2007).
5. Q. Li, M. L. Onozato, P. M. Andrews, C. W. Chen, A. Paek, R. Naphas, S. Yuan, J. Jiang, A. Cable, and Y. Chen, "Automated quantification of microstructural dimensions of the human kidney using optical coherence tomography (OCT)," Opt. Express **17**(18), 16000–16016 (2009).
6. G. Popescu, L. P. Deflores, J. C. Vaughan, K. Badizadegan, H. Iwai, R. R. Dasari, and M. S. Feld, "Fourier phase microscopy for investigation of biological structures and dynamics," Opt. Lett. **29**(21), 2503–2505 (2004).
7. G. Popescu, Y. Park, N. Lue, C. Best-Popescu, L. Deflores, R. R. Dasari, M. S. Feld, and K. Badizadegan, "Optical imaging of cell mass and growth dynamics," Am. J. Physiol. Cell Physiol. **295**(2), C538–C544 (2008).
8. G. Popescu, T. Ikeda, R. R. Dasari, and M. S. Feld, "Diffraction phase microscopy for quantifying cell structure and dynamics," Opt. Lett. **31**(6), 775–777 (2006).
9. F. Merola, L. Miccio, P. Memmolo, G. Di Caprio, A. Galli, R. Puglisi, D. Balduzzi, G. Coppola, P. Netti, and P. Ferraro, "Digital holography as a method for 3D imaging and estimating the biovolume of motile cells," Lab Chip **13**(23), 4512–4516 (2013).
10. P. Memmolo, M. Iannone, M. Ventre, P. A. Netti, A. Finizio, M. Paturzo, and P. Ferraro, "On the holographic 3D tracking of in vitro cells characterized by a highly-morphological change," Opt. Express **20**(27), 28485–28493 (2012).

#319886 https://doi.org/10.1364/BOE.9.000921
Journal © 2018 Received 13 Oct 2017; accepted 25 Jan 2018; published 1 Feb 2018

Biomedical Optics EXPRESS

11. P. Memmolo, G. Di Caprio, C. Distante, M. Paturzo, R. Puglisi, D. Balduzzi, A. Galli, G. Coppola, and P. Ferraro, "Identification of bovine sperm head for morphometry analysis in quantitative phase-contrast holographic microscopy," Opt. Express **19**(23), 23215–23226 (2011).
12. G. Di Caprio, M. A. Gioffre, N. Saffioti, S. Grilli, P. Ferraro, R. Puglisi, D. Balduzzi, A. Galli, and G. Coppola, "Quantitative Label-Free Animal Sperm Imaging by Means of Digital Holographic Microscopy," IEEE J. Sel. Top. Quantum Electron. **16**(4), 833–840 (2010).
13. P. Memmolo, L. Miccio, A. Finizio, P. A. Netti, and P. Ferraro, "Holographic tracking of living cells by three-dimensional reconstructed complex wavefronts alignment," Opt. Lett. **39**(9), 2759–2762 (2014).
14. G. Coppola, G. Di Caprio, M. Wilding, P. Ferraro, G. Esposito, L. Di Matteo, R. Dale, G. Coppola, and B. Dale, "Digital holographic microscopy for the evaluation of human sperm structure," Zygote **22**(4), 446–454 (2014).
15. M. Paturzo, A. Finizio, P. Memmolo, R. Puglisi, D. Balduzzi, A. Galli, and P. Ferraro, "Microscopy imaging and quantitative phase contrast mapping in turbid microfluidic channels by digital holography," Lab Chip **12**(17), 3073–3076 (2012).
16. P. Memmolo, A. Finizio, M. Paturzo, L. Miccio, and P. Ferraro, "Twin-beams digital holography for 3D tracking and quantitative phase-contrast microscopy in microfluidics," Opt. Express **19**(25), 25833–25842 (2011).
17. V. Bianco, M. Paturzo, A. Finizio, D. Balduzzi, R. Puglisi, A. Galli, and P. Ferraro, "Clear coherent imaging in turbid microfluidics by multiple holographic acquisitions," Opt. Lett. **37**(20), 4212–4214 (2012).
18. F. Merola, L. Miccio, M. Paturzo, A. Finizio, S. Grilli, and P. Ferraro, "Driving and analysis of micro-objects by digital holographic microscope in microfluidics," Opt. Lett. **36**(16), 3079–3081 (2011).
19. V. Bianco, M. Paturzo, O. Gennari, A. Finizio, and P. Ferraro, "Imaging through scattering microfluidic channels by digital holography for information recovery in lab on chip," Opt. Express **21**(20), 23985–23996 (2013).
20. D. Dannhauser, D. Rossi, F. Causa, P. Memmolo, A. Finizio, T. Wriedt, J. Hellmers, Y. Eremin, P. Ferraro, and P. A. Netti, "Optical signature of erythrocytes by light scattering in microfluidic flows," Lab Chip **15**(16), 3278–3285 (2015).
21. M. Matrecano, M. Paturzo, A. Finizio, and P. Ferraro, "Enhancing depth of focus in tilted microfluidics channels by digital holography," Opt. Lett. **38**(6), 896–898 (2013).
22. M. Shan, M. E. Kandel, and G. Popescu, "Refractive index variance of cells and tissues measured by quantitative phase imaging," Opt. Express **25**(2), 1573–1581 (2017).
23. E. Min, M. E. Kandel, C. J. Ko, G. Popescu, W. Jung, and C. Best-Popescu, "Label-free, multi-scale imaging of ex-vivo mouse brain using spatial light interference microscopy," Sci Rep **6**, 39667 (2016).
24. M. Lee, E. Lee, J. Jung, H. Yu, K. Kim, J. Yoon, S. Lee, Y. Jeong, and Y. Park, "Label-free optical quantification of structural alterations in Alzheimer's disease," Sci Rep **6**, 31034 (2016).
25. M. Mir, Z. Wang, Z. Shen, M. Bednarz, R. Bashir, I. Golding, S. G. Prasanth, and G. Popescu, "Optical measurement of cycle-dependent cell growth," Proc. Natl. Acad. Sci. U.S.A. **108**(32), 13124–13129 (2011).
26. E. Min, S. Ban, Y. Wang, S. C. Bae, G. Popescu, C. Best-Popescu, and W. Jung, "Measurement of multispectral scattering properties in mouse brain tissue," Biomed. Opt. Express **8**(3), 1763–1770 (2017).
27. Z. Wang, K. Tangella, A. Balla, and G. Popescu, "Tissue refractive index as marker of disease," J. Biomed. Opt. **16**(11), 116017 (2011).
28. S. Sridharan, V. Macias, K. Tangella, A. Kajdacsy-Balla, and G. Popescu, "Prediction of prostate cancer recurrence using quantitative phase imaging," Sci Rep **5**, 9976 (2015).
29. H. Majeed, C. Okoro, A. Kajdacsy-Balla, K. C. Toussaint, Jr., and G. Popescu, "Quantifying collagen fiber orientation in breast cancer using quantitative phase imaging," J. Biomed. Opt. **22**(4), 046004 (2017).
30. B. Bhaduri, C. Edwards, H. Pham, R. J. Zhou, T. H. Nguyen, L. L. Goddard, and G. Popescu, "Diffraction phase microscopy: principles and applications in materials and life sciences," Adv. Opt. Photonics **6**(1), 57–119 (2014).
31. C. Edwards, A. Arbabi, G. Popescu, and L. L. Goddard, "Optically monitoring and controlling nanoscale topography during semiconductor etching," Light Sci. Appl. **1**, e30 (2012).
32. H. V. Pham, C. Edwards, L. L. Goddard, and G. Popescu, "Fast phase reconstruction in white light diffraction phase microscopy," Appl. Opt. **52**(1), A97–A101 (2013).
33. J. A. Collett, D. O. Traktuev, P. Mehrotra, A. Crone, S. Merfeld-Clauss, K. L. March, and D. P. Basile, "Human adipose stromal cell therapy improves survival and reduces renal inflammation and capillary rarefaction in acute kidney injury," J. Cell. Mol. Med. **21**(7), 1420–1430 (2017).
34. M. S. Paller, J. R. Hoidal, and T. F. Ferris, "Oxygen free radicals in ischemic acute renal failure in the rat," J. Clin. Invest. **74**(4), 1156–1164 (1984).
35. Z. Wang, H. Ding, and G. Popescu, "Scattering-phase theorem," Opt. Lett. **36**(7), 1215–1217 (2011).
36. T. Shimokawa, H. Tsutsui, T. Miura, T. Nishinaka, T. Terada, M. Takama, S. Yoshida, T. Tanba, A. Tojo, M. Yamagata, and T. Yukimura, "Renoprotective effect of yohimbine on ischaemia/reperfusion-induced acute kidney injury through alpha2C-adrenoceptors in rats," Eur J Pharmacol **781**, 36–44 (2016).
37. G. Popescu, Y. Park, W. Choi, R. R. Dasari, M. S. Feld, and K. Badizadegan, "Imaging red blood cell dynamics by quantitative phase microscopy," Blood Cells Mol. Dis. **41**(1), 10–16 (2008).
38. R. W. Schrier, W. Wang, B. Poole, and A. Mitra, "Acute renal failure: definitions, diagnosis, pathogenesis, and therapy," J. Clin. Invest. **114**(1), 5–14 (2004).

Biomedical Optics EXPRESS

1. Introduction

Acute kidney injury (AKI) is characterized by sudden loss of renal ability of wasting materials from the blood. In order to verify the abnormalities caused by AKI, the renal histopathological study has been investigated based on standard hematoxylin and eosin (H&E) staining or selectively labeled-tagging molecules with specific immuno-histochemical stains. Failure of accurate prediction of kidney damage and alterations associated with AKI represents a major clinical problem. Thus, it is very important to quantitatively track the tissue deterioration during disease progression. Existing imaging methods for the kidney study include magnetic resonance imaging (MRI) and positron emission tomography (PET), which have a limited low spatial resolution of around 100 μm [1]. Micro computed tomography (μCT) can achieve higher spatial resolution up to 1 μm, and is currently being used in order to quantify blood vessel architecture in kidney ex vivo. However, it requires adequate amount of contrast agent [2]. Histological imaging technique for sliced thin tissue in 4 – 5 μm has been the gold standard for diagnosis of renal failure ranging from the subcellular scale to several millimeter scale. However, this approach requires manual investigation by a pathologist, and the result brings about only qualitative analysis. Furthermore, high contrast fluorescence imaging of endogenous/exogenous fluorophores has been used in addressing progressive renal tubule-interstitial fibrosis, but this type of imaging also requires many steps of sample preparation [3]. Complementary label-free imaging techniques, such as optical coherence tomography (OCT) were employed in renal studies due to its relatively high penetration depth [4, 5]. However, they only provide a limited information of sample characteristic such as morphology and anatomical feature. Recently, quantitative phase imaging (QPI) has emerged as a new tool for measuring refractive index distribution in various types of cell membrane including, i.e., neurons, HeLa, bovine/human sperm, red blood cell (RBC), etc [6–14]. QPI has also demonstrated its great potential to be used in turbid media combined with microfluidic channel [15–21], and in tissue level with nanoscale sensitivity [22–24]. Complex optical fields measured by interferometry can be employed in many biological applications by calculating optical parameter including dry mass density and refractive index (RI) of tissues [25]. Using RI values from different types of tissue, optical parameter of scattering coefficient and anisotropy highlight unique tissue characteristics [26, 27]. Not only to normal tissues, QPI has also showed great possibility for uncovering tissue properties in disease models such as prostate and breast cancer [28, 29].

Here, we present a label-free approach to quantitatively measure optical properties of acute kidney disease. Diffraction phase microscopy (DPM) [30] equipped with XY motorized stages is a wide-field QPI technique which allows for the label-free visualization of the kidney anatomy over broad spatial scales. It demonstrates that our method shed light on previously unknown tissue properties affected by renal disease. In particular, AKI, one of the typical renal diseases, was investigated in terms of phase delay, retrieved scattering coefficient (μ_s) and anisotropy (g). Compared to healthy kidney tissue, we observed altered anatomical structure and optical parameter distribution in the disease model. Our results show that the label-free DPM technique provides great capability as a valuable tool complement to existing gold standard in pathophysiology of AKI and nephrology.

2. Materials and method

2.1 Sample preparation

All animal procedures were carried out in accordance with the recommendations in the Guide for the Care and Use of Laboratory Animals of the National Institutes of Health. The animal protocol was approved by Animal Care and Use Committee in Ulsan National Institute of Science and Technology (UNIST IACUC-15-27). All experiments were conducted using 8 weeks old male C57BL/6 mice. The mice were sacrificed after deep anesthetization by intraperitoneal injection of Zoletil (30 mg/kg) and Rompun (10 mg/kg) mixture. Then, the

Biomedical Optics EXPRESS

kidney sample that was transcardially perfusion-fixed were incubated in 10% neutral buffered formalin for 24 hours at 4°C, and dehydrated through graded ethanol and xylene, and infiltrated with paraffin wax. The paraffin embedded kidney sample was dissected out along the coronal plane with thickness of 5 μm by microtome (catalog no. RM2255. Leica). Every histological sections of the mouse kidney were prepared according to the standard procedures. Prior to imaging, the paraffin was completely removed by washes with xylene and graded

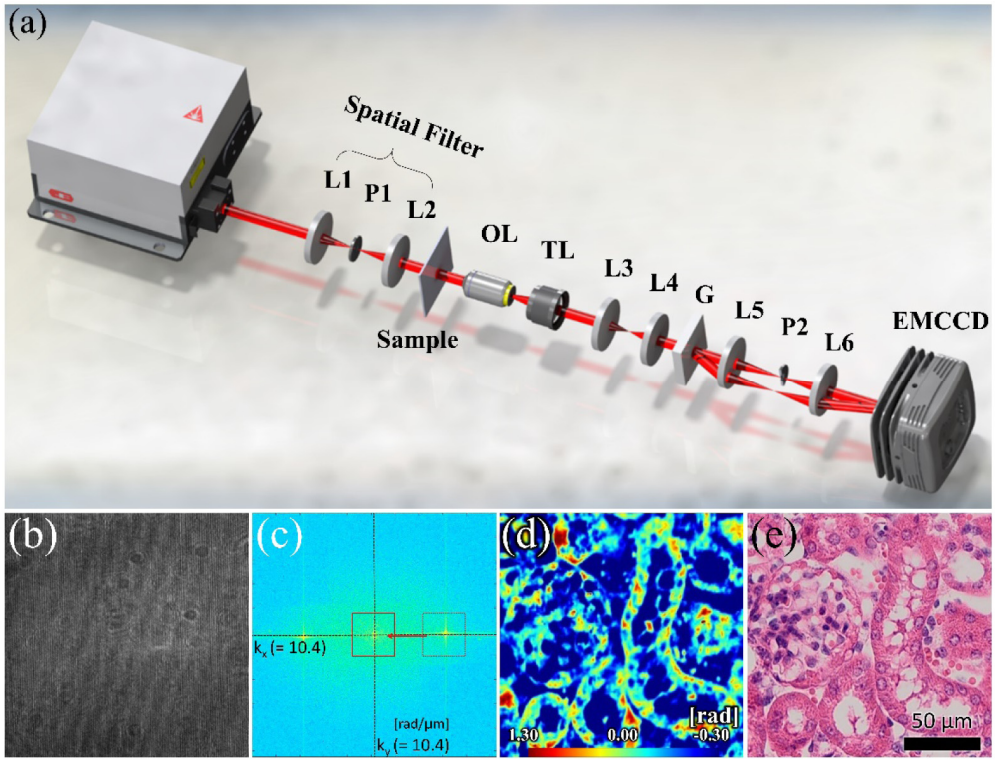

Fig. 1. Experimental set-up and phase delay image reconstruction. (a) Schematic of the DPM optical set up using with long-range XY scanning stages and detailed optical path. (b) Measured raw interferogram. (c) Spatial frequency domain spectrum of (b). The first order (rectangular box) is shifted to the origin, an operation that is based on Hilbert transform. (d) Retrieved QPI of kidney tissue imaged in (b). (e) Corresponding H&E stained tissue.

ethanol. After DPM analysis, the samples were stained with hematoxylin and eosin dye according to standard procedure. The corresponding sections were imaged by virtual microscope slide scanning system (.slide, OLYMPUS) for comparison.

2.2 Acute kidney injury model

The mice were anesthetized with Zoletil (30 mg/kg) and Rompun (10 mg/kg) mixture. After haircut, right kidney was exposed through the site of the right flank incision. Ischemia/reperfusion injury was induced for 30 min by clamping renal pedicle with nontraumatic micro-aneurysm clamp (Roboz Surgical Instruments, Washington, DC). When clamp were removed, reperfusion was confirmed completely. Then, sham-operated mice underwent the same surgical procedure except for the renal pedicle clamping. And, the mice were sacrificed at 0, 3, 5, 7 days after procedure for a dynamic monitoring of disease progression of I/R injury.

Biomedical Optics EXPRESS

2.3 Imaging

As shown in Fig. 1(a), DPM set up was built based on common-path and off-axis interferometry [30]. With motorized long-range enabled stages for XY scanning, it enabled imaging entire coronal section of the mouse kidney. For the illumination source, broadband white light laser (Fianium, WhiteLase SC-400) was used. Optical filters (Delta optical thin film, LVNIRBP) were placed for the purpose of specific wavelength selection in this case of 550 nm. After passing through by two lens (L1/L2) and pinhole (P1), beam is spatially filtered to produce a clean Gaussian beam. To acquire high resolution image in wide field and in multi-scale, we used a 40 × objective lens (OL, Olympus, UMPlanFl NA 0.8) and a 200 mm tube lens (Thorlabs, ITL200). The diffraction grating (G) (Edmond, 92 grooves/mm) was placed at the image plane, and the light field is divided by diffraction orders. The 0th and 1st order were used as reference and sample beam, respectively. The two beams pass through the lens (L5) and only the 0th beam is spatially filtered at the Fourier plane (FP) by the pinhole (P2), of 50 μm radius. The reference and sample beams are collected by the next lens (L6) such that they make interference at the EMCCD (Andor, iXon3). Each recorded individual interferogram was used to extract the phase information. Using field-retrieval algorithm [30], we took the Fourier transform of raw interferogram, and a simple bandpass filter was used to select spatially modulated first-order and shifted back to baseband (Fig. 1(b) and 1(c)). For the background subtraction, image complex field was divided by its calibration image complex field [31, 32], which was acquired in the no-sample region. The field of view (FOV) for single tile image is 150 x 150 μm^2 which overlaps 25% with adjacent images. Automatic plugin stitching function in ImageJ tool was used to reconstruct a wide-field phase image having the total FOV of 7.9 x 5.8 mm from 7,416 mosaic tiles (72 x 103) for Fig. 2(a), with total imaging time of ~30 minutes. Acquisition rate of DPM system was measured to be 5 frame/sec. In order to prevent any unnecessary motion artifact, motorized linear stages was set to wait 200 ms till a single image acquisition of EMCCD is completed. By measuring the phase differences from the specimen and surrounding mounting agent over whole area of sectioned kidney, the entire phase delay images were achieved. The reconstructed image represent the phase delay due to its spatial alteration and difference of refractive index of tissue (Fig. 1(d)). The more detailed phase image reconstruction method using interference pattern was described in [30], Bhaduri et al. The spatial and temporal phase stability of the system was measured to be 40 and 50 mrad. The transverse resolution was 1.2 μm at the wavelength of 550 nm.

3. Result

3.1 Quantitative phase imaging of renal cortex, medulla, and pelvis

We obtained DPM images of kidney in a coronal section as shown in Fig. 2. The corresponding H&E stained image are also presented for a side by side comparison. DPM reveals detailed information about the architecture of renal tissue. In order to delineate internal region of kidney slice at macro-scale, we applied the background thresholding only in wide-field imaging as shown in Fig. 2(a), whereas rest of other magnified structures of Fig. 2(b)-2(e) were visualized in raw data without any thresholding process. This bean-shaped organ is divided into three main internal regions: outer renal cortex, medulla in middle, and pelvis in inner area (Fig. 2(a)). The renal cortex coats the outside of kidney where groups of nephrons are distributed. The nephron is the basic structural and functional unit being composed of different types of tubules, including the proximal convoluted tubule (PCT) (Fig. 2(c3)), distal convoluted tubule (DCT) (Fig. 2(c4)) and renal corpuscle (Fig. 2(c1)). As shown in Fig. 2, PCT has higher phase variance value than the other types of tubule. This is because PCT has brush border, which is densely packed with microvilli. While PCT looks occluded, DCT has relatively clean border inside, resulting in less phase variance value. Another component of the nephron is the renal corpuscle, which consists of two structures like a

Biomedical Optics EXPRESS

glomerulus and a Bowman's capsule. The main role of the renal corpuscle is to make blood filtration and regulate blood flow. The renal corpuscle retains a tuft of micro-capillaries, endothelial cells, and mesangial cells. Since renal corpuscles need to play the role of filtration, the endothelial cell in glomerulus has large fenestrae, a number of small pore-like structures in the cell. These porous structures can be easily attacked and damaged depending on renal dysfunction and a variety of genetic and environmental causes, which affect the higher phase variance in glomerulus.

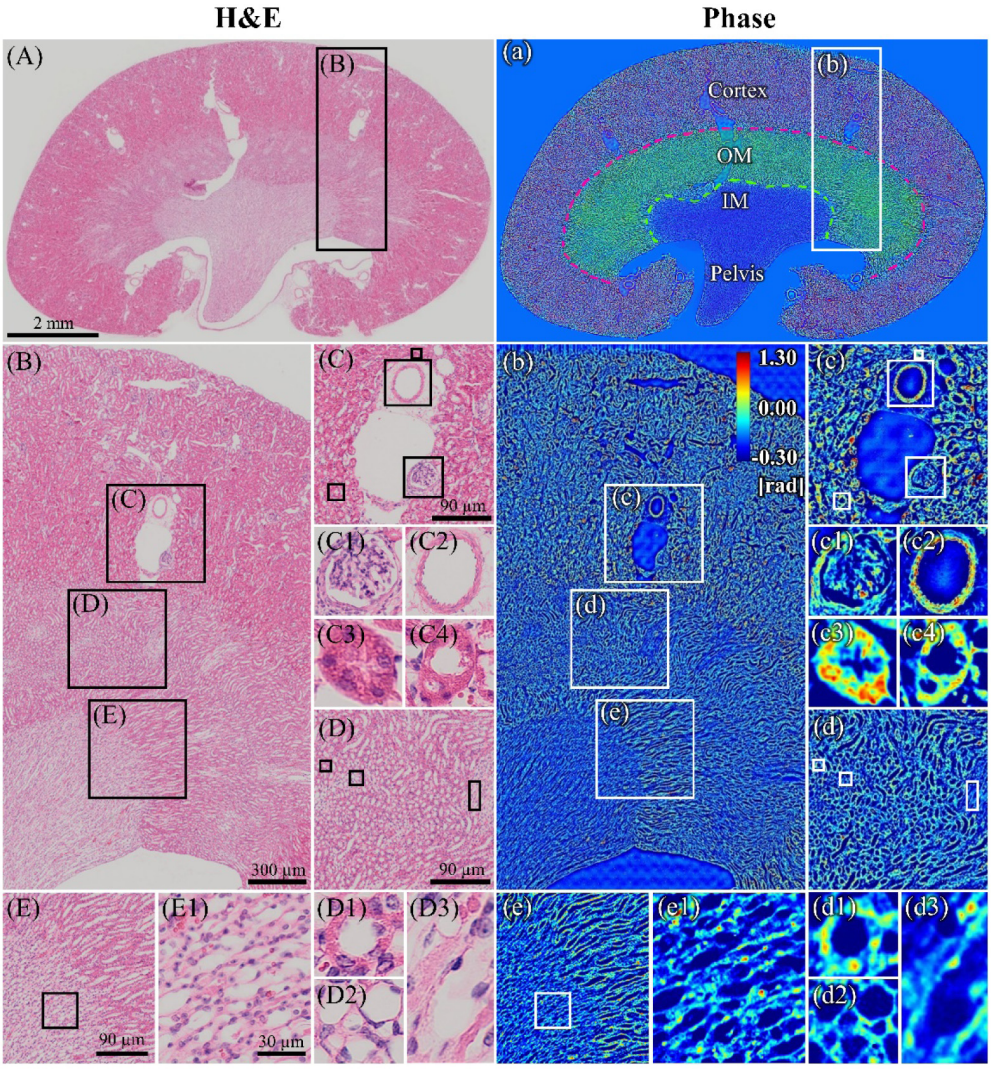

Fig. 2. H&E and DPM imaging of a mouse kidney tissue in coronal way. Entire wide-field imaging of the kidney tissue slice is presented on the left (A) and right column (a) for H&E and DPM, respectively. Major regions was denoted with different color shade in (a). Black boxes in the H&E stained images denote specific anatomical components in various layers. The same regions denoted by white boxes in the DPM images. These insets include: renal cortex (C/c), outer medulla (D/d), boundary between inner medulla and pelvis (E/e). Glomerular Capsule, renal capillaries, proximal convoluted tubule, and distal convoluted tubule in the cortex are presented in C1/c1, C2/c2, C3/c3, and C4/c4, respectively. Medullary components of the thick loop of Henle, thin loop of Henle, and collecting tubule are shown in D1/d1, D2/d2 and D3/d3, respectively. A group of collecting duct has been delineated in E1/e1.

Biomedical Optics EXPRESS

Underneath the cortex, the renal medulla is found at the center of the kidney. This part of the kidney also consists of different types of vessels and tubules, including vasa recta, interstitium, loop of Henle, and medullary collecting ducts. Nephrons are not only located in the cortex, but also extend to medulla. The unique spatial arrangement of the nephron component makes medulla more crucial for urine concentration and other specialized kidney functions. As shown in Fig. 2(d), the medullary region is clearly visualized, corresponding closely to the H&E stained image. The thick and thin limb of loop of Henle was shown in detailed (Fig. 2(d1) and 2(d2)). As indicted from the name of each tubule, thick limb of loop

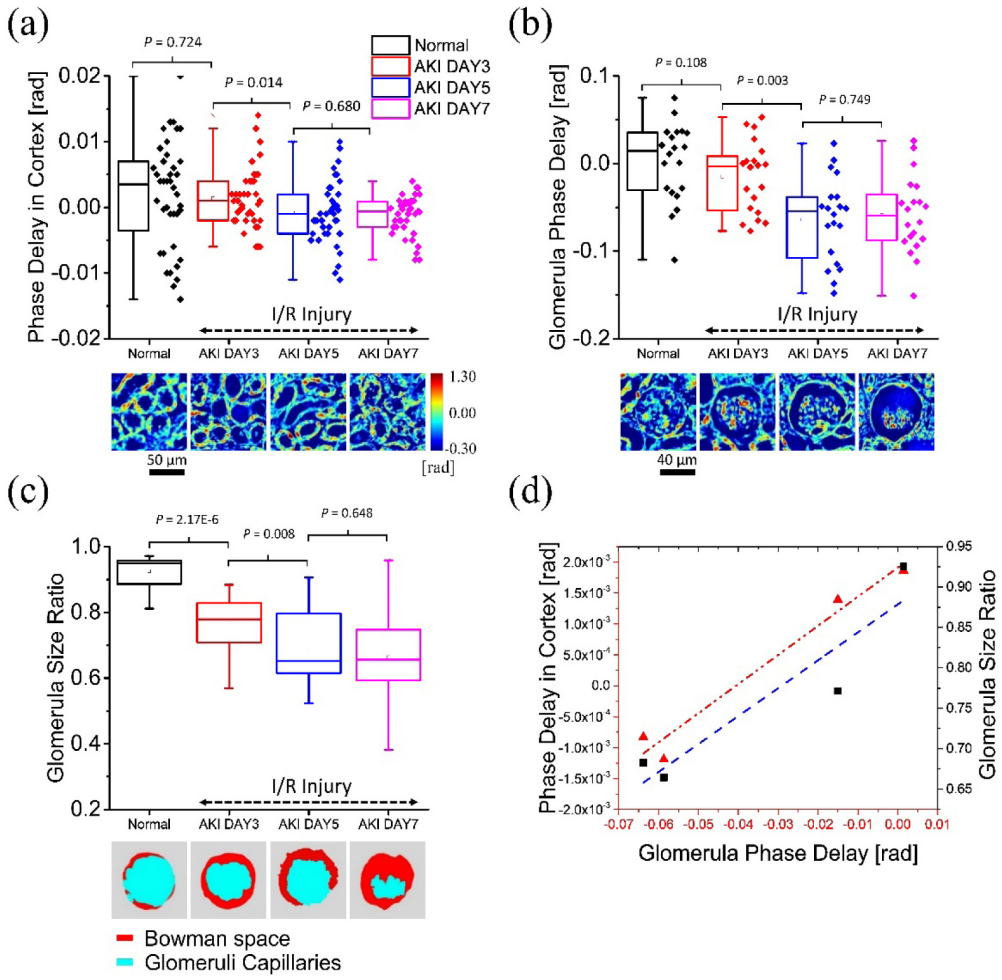

Fig. 3. (a) Phase delay of kidney cortex region after 0, 3, 5 and 7 day of AKI. (b) Glomerular phase delay in cortex after 0, 3, 5 and 7 day of AKI. Inset of each stage in (a) and (b) represents one of the randomly selected phase map. Box plot is made by average of each map. The box covers the 25–75% percentiles representing the standard deviation of averaged phase maps, and the maximum length of whisker is 2 times the standard deviation. (c) The size ratio of capillary to a single glomerular capsule. Glomerular capillaries are segmented out of bowman's space as shown in inset of (c). (d) Linear fit between phase delay in cortex and glomerular phase delay (red), same study between glomerular size ratio and glomerular phase delay (blue).

of Henle shows higher phase variance due to its spatial thickness. And medullary collecting duct in medulla concentrates and transports urine from the nephrons and moves it into the renal pelvis and ureters. This structure is relatively easier to distinguish from the other tubules

Biomedical Optics EXPRESS

since it has a long and narrow appearance. Since it also shows low value of phase variance, this type of tubule can be readily delineated among other types of tubules.

Renal pelvis is area that collects urine from the end part of nephron and narrows into the upper end of the ureter. Most region of pelvis comprised of collecting tubules and papillary ducts. As shown in Fig. 2(e), the boundary between inner part of the medulla and pelvis is clearly visualized. A group of collecting ducts exist in elongated way shown in Fig. 2(e1) with relatively low phase value.

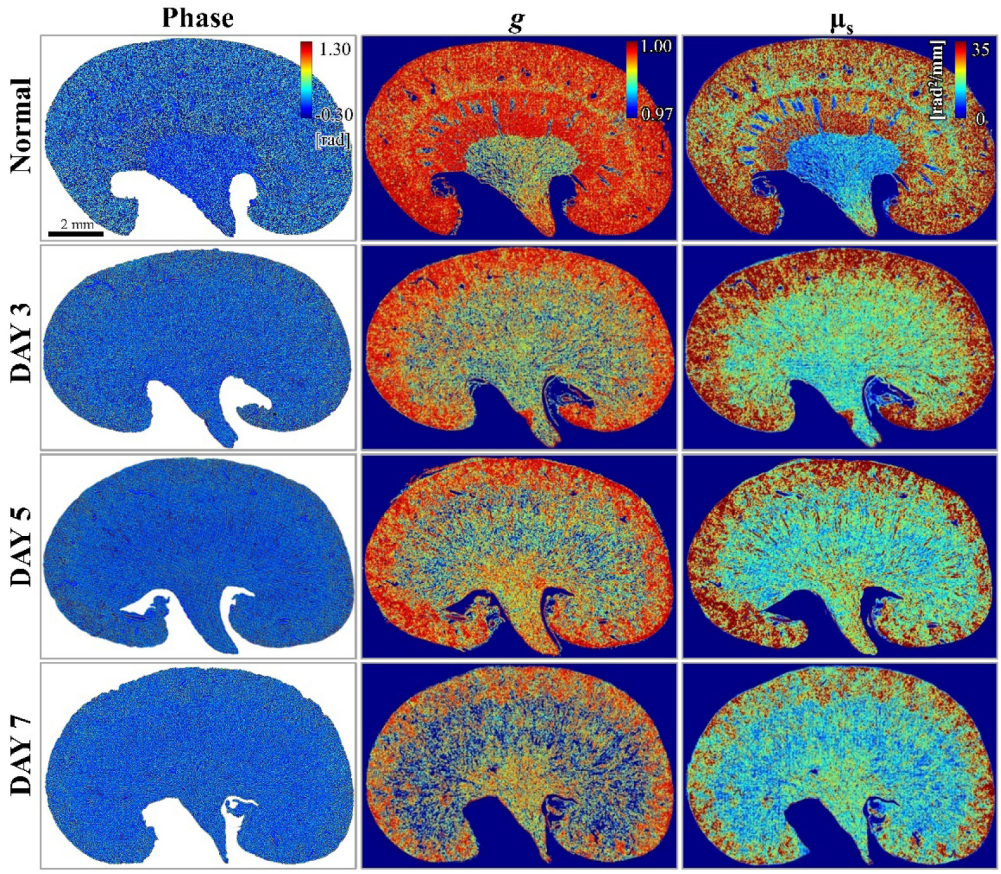

Fig. 4. Optical parameter maps associated with the kidney tissue slice obtained from the quantitative phase image. Phase delay image of kidney coronal slice for AKI model in time scale (first column). Remapped with g (second column) and μ_s (third column) for the same kidney sample.

3.2 Fluctuations of phase values and glomerular size in renal cortex during AKI development

In Fig. 3, we analyzed and tracked how this disease makes morphological and functional alterations to the renal cortex. Previously, it was known that the cortex region is the first area that is severely deteriorated due to renal tubule-interstitial fibrosis [33]. Renal fibrosis is a progressive process that leads to tissue scarring and architectural change. Thus, we obtained phase maps from the renal cortex region and glomerular to make graph of Fig. 3(a) and 3(b). Specifically, we obtained 40 for phase delay and 20 for glomerulus from each AKI stage and averaged for each map. Then, we draw a box plot about randomly selected average phase values for each stage. The inset figures of Fig. 3(a) and 3(b) represents phase map of each stage we randomly picked in renal cortex and glomerular, respectively. The raw data besides

Biomedical Optics EXPRESS

to box plot represents an averaged value of each phase map. It is found that the phase variance in the renal cortex is decreased from normal to DAY 7 (Fig. 3(a)). The altered geometrical shapes and spatial inhomogeneity induced by ischemic stress makes lower phase variance value in day 7. We confirmed that the phase variance of the glomeruli in renal cortex decreased due to relatively increased Bowman's space surrounding the Glomeruli capillaries (Fig. 3(b)). Glomerular capsule consists of two sub components, glomerular capillary and Bowman's space, respectively. As AKI develops, blood flow into glomerular is decreased

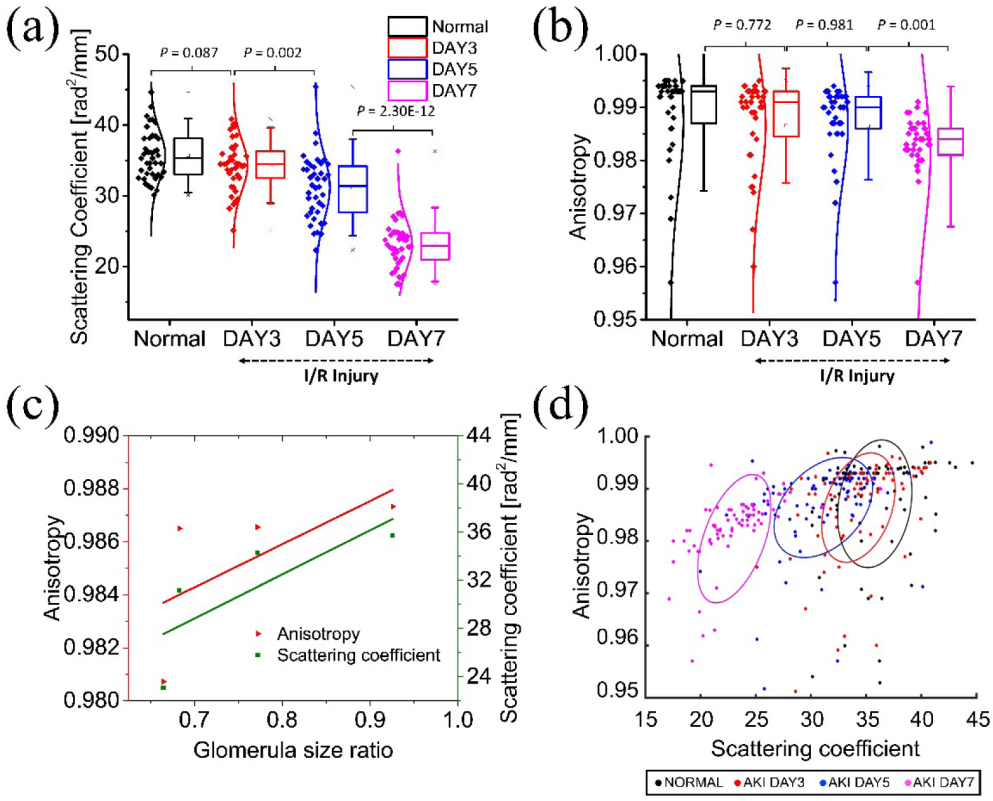

Fig. 5. AKI prognosis through optical properties. The u_s and g retrieved based on scattering-phase theorem, as described in text. (a) Plot of quantitatively calculated μ_s of renal cortex in time scale of AKI. (b) Plot of quantitative g in same time scale of AKI. The μ_s and g both are plotted using box plot. The box covers the 25–75% percentiles representing standard deviation, and the maximum length of whisker is 2 times the standard deviation. (c) Linear fit between geometrical information of glomerular capillary size and g in cortex region (red), and between size of glomerular capillaries and μ_s (green). (d) Density contour plot of optical properties of AKI mode.

resulting to glomerular capillary congestion and acute tubular necrosis [34]. Not only phase value of glomeruli, but also the size of glomerular capillary was evaluated because it is important risk factor in renal fibrosis diagnosis (Fig. 3(c)). It demonstrates that the size of glomerular capillary was decreased while Bowman's space is increased. For the correlation study between three factors of phase delay in the cortex, phase delay in glomerular, and glomerular capillary size, respectively, we plotted their correlative linear relationship as shown in Fig. 3(d). Phase information in the cortex and glomerular show significant correlation with high value of Pearson's r value (red dot line). Similarly, correlation linear fit study between glomerular phase delay and size is analyzed with blue line. Through correlation analysis, it reflects that renal damage in cortex region is related to the phase fluctuation and the size of glomerular capillaries.

Biomedical Optics EXPRESS

3.3 AKI scattering coefficient and anisotropy

DPM delineates morphological information with nanometer sensitivity, but the phase value does not provide sufficient macroscopic contrast which determines the progress of interstitial fibrosis. Thus, we quantitatively calculated its optical scattering parameters, namely the scattering coefficient (μ_s) and anisotropy (g) using the complex field information [35]. μ_s can be described by light intensity

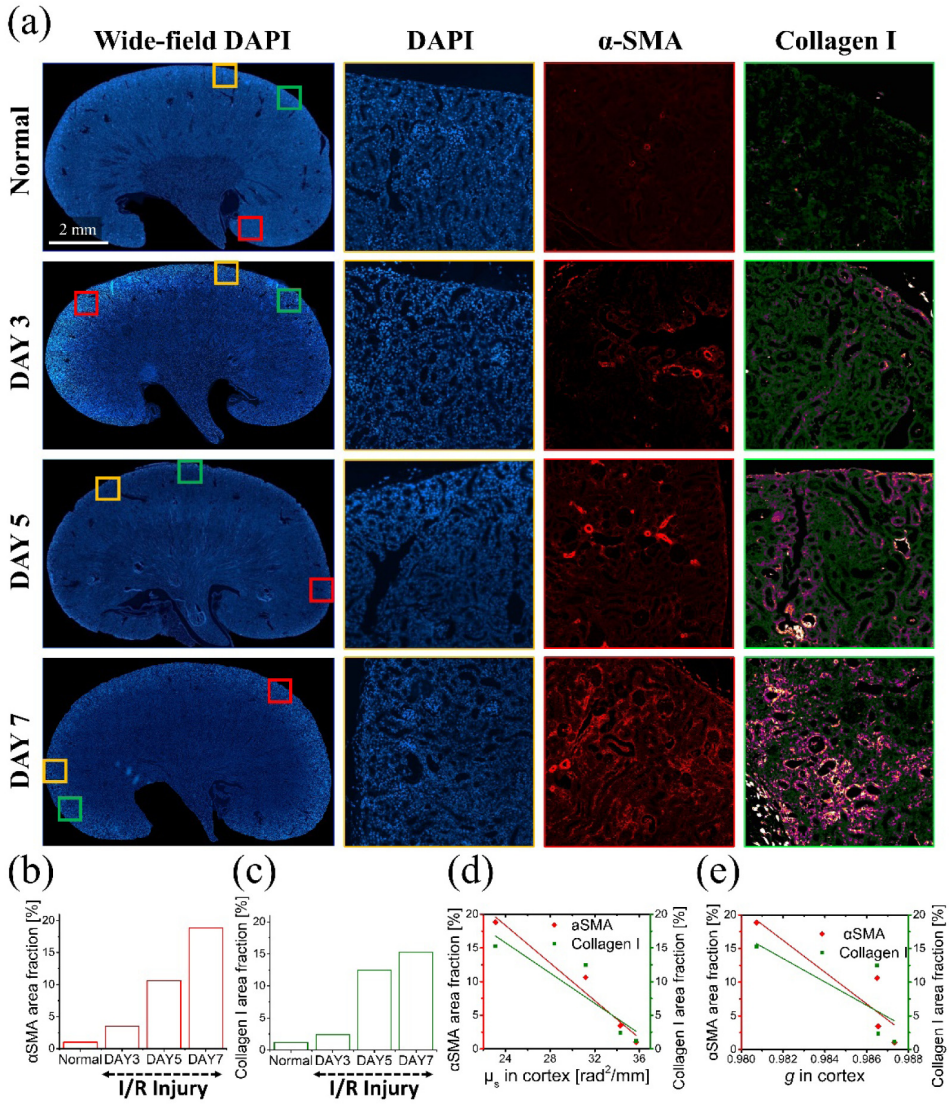

Fig. 6. Area fraction in capillary is closely associated with renal fibrosis in I/R-induced progressive kidney fibrosis. (a) Immunohistochemistry of DAPI in wide field, and magnified cortex region of DAPI, α-SMA, and collagen I in time scale of AKI. (b) Time course of quantified positively stained area fractions for α-SMA and (c) collagen I. (d) Significant correlations were found between the computationally filled α-SMA area fraction and scattering coefficient in renal cortex (red), and also found between collagen I and scattering coefficient in renal cortex (green). (d) Another significant correlations were found between the computationally filled α-SMA area fraction and anisotropy in renal cortex (red), and also found between collagen I and anisotropy in renal cortex (green).

Biomedical Optics EXPRESS

attenuation per unit distance. From the phase delay, the scattering coefficient (μ_s) (Fig. 5(a)) can be retrieved based on the scattering-phase theorem.

$$\mu_s = \frac{\left\langle \Delta\phi^2(r) \right\rangle_r}{L} \tag{1}$$

$\left\langle \Delta\phi^2(r) \right\rangle_r$ indicates spatial variance of the phase $\phi(r)$, which can be calculated by $\left\langle \left[\phi(r) - \left\langle \phi(r) \right\rangle_r \right]^2 \right\rangle_r$ with windows size of 2.9 x 2.9 um^2 where < >r denotes spatial average. L is the thickness of kidney slice which has 5 μm in this case. Since it is sensitive to geometrical arrangement, various cell types, and subcellular compositions in the tissue, it reflect the relationship between spatial alteration and scattering field. The area with the highest values of μ_s corresponds to high local contrast of refractive index (RI). The renal cortex and outer medullar exhibit higher scattering coefficient than the other sub-regions primarily due to the presence of a group of dense PCT. The densely packed microvilli in brush border of PCT may relate to high scattering value in the cortex. Since the renal dysfunction occurs with gradual development of glomerulosclerosis and interstitial fibrosis, renal tubules and interstitial capillaries are destructed are destructed during AKI development [36], which result in the low scattering value as shown in Fig. 4. As shown in Fig. 5(a), the corresponding μs value is decreased, and this result reflects significant effect of interstitial fibrosis on spatial alteration in cortex region.

The other critical optical parameter is anisotropy (g). *g* can be retrieved by the average of the cosine of the scattering angle, and has the single directionality of forward scattering. Anisotropy can be calculated through the following equation using scattering phase theorem [35].

$$g = 1 - \frac{1}{2k_o^2} \frac{\left\langle \left| \nabla \left[\phi(r) \right] \right|^2 \right\rangle_r}{\left\langle \Delta\phi^2(r) \right\rangle_r^2} \tag{2}$$

Where n_0 and λ_0 are the average refractive index and the average wavelength of light in the kidney tissue, k_0 (= $2\pi n_0/\lambda_0$) is the incident wave vector, and $\nabla[\varnothing(r)]$ is the phase gradient, respectively. This equation indicates that the anisotropy factor is related to the scattering coefficient, as well as the phase gradient that is associated with the tilt in the direction of propagation. As shown in Fig. 4, mapped distribution of g exhibits a value ranging from 0.9 to 1, which is analogous to other types of tissues [37]. In healthy mice, high g is found in renal cortex mainly due to the large size of scattering particles. Though the g value is high in normal with median value of 0.994, it gradually decreases as kidney get injured by ischemic stress as shown in Fig. 5(b). In order to check the correlation between two different optical properties and geometrical information of glomerular capillaries, linear fitting was computed and plotted as shown in Fig. 5(c). These analysis exhibit adequate correlation of μ_s and g in renal cortex about the gradual renal fibrosis of AKI with Pearson's r value of 0.77 and 0.63, respectively. Eventually, low μ_s and g value in day 7 of AKI represent high tissue homogeneity and small scattering particles mostly induced by tubuolo-interstitial fibrosis in renal cortex. And, density contour plot of scattering and anisotropy clearly distinguished their distinct distribution showing better discrimination from normal to day 7 (Fig. 5(d)).

3.4 Renal fibrosis is closely associated with optical characteristics of μ_s and g

Renal fibrosis in AKI can be confirmed through immunohistochemical (IHC) study. For comparison, we used a tissue slice adjacent to the DPM image slice for IHC. A continuous increase of positive fibroblast from α-smooth muscle actin (αSMA) and collagen I confirmed

Biomedical Optics EXPRESS

the development of progressive fibrosis (Fig. 6(a)). Positively stained area fractions for αSMA and collagen I represent the reconstructed neo-vascular area, which is one of the major renal fibrosis indicator (Fig. 6(b) and 6(c)). In addition, significant correlations were found between the computationally filled area fractions for αSMA and collagen I, illustrating a close association between renal fibrosis and optical properties of μ_s and g. (Fig. 6(d) and 6(e)). High Pearson's r value between fibrosis and μ_s, and between fibrosis and g explains the potential of QPI as a reliable tool for kidney pathophysiology

4. Discussion and conclusion

Ischemic stress damage to the cortex and causes a decreased renal blood flow from major renal artery, which eventually brings about renal dysfunction, and a series of inflammatory process in extra cellular matrix, ending up with developing chronic kidney disease (CKD) [38]. There has been no label free technique for detecting the tubule-interstitial fibrogenetic injury quantitatively in large-scale. Using DPM, we developed a new approach for generating high resolution images of ex-vivo mouse kidney in multi-scale with high phase stability and sensitivity. We demonstrated wide-field label free analysis for detecting the progressive renal disease for the first time. Using a mosaic platform equipped with XY motorized linear stages, wide field quantitative phase image with an image-mosaicking technique were acquired. In order to delineate macroscopic contrast on renal fibrosis, we retrieved light scattering parameters, i.e., scattering coefficient (μ_s) and anisotropy (g). The results suggest that this approach can be applied to systematically quantify the structural alteration of AKI pathophysiology by measuring quantitative phase delay of kidney slices. The μ_s and g retrieved by 2D phase image showed a great potential on detecting interstitial fibrosis, which H&E staining, gold standard of kidney pathology, cannot offer. The contrast generated from optical properties showed a good agreement with previously reported result of IHC study addressed by αSMA and collagen I. The correlative result between optical parameters and fibrogenetic marker supports the efficacy of DPM as a versatile tool for describing the prognosis of AKI.

Funding

National Research Foundation of Korea (NRF) grant from Korea government (MSIP) (No. 2017009566); and 2017 Research Fund (1.170009) of UNIST (Ulsan National Institute of Science & Technology).

Acknowledgements

We would like to thank Sung Chul Bae and Sung Ho Lee for technical assistance.

Disclosures

The authors declare that there are no conflicts of interest related to this article.